JOURNAL OF CATALYSIS 143, 227–238 (1993)

Crystalline Microporous MAPO-36 Molecular Sieve: Synthesis and Characterization

DEEPAK B. AKOLEKAR

Department of Chemical Engineering, University of Laval, Ste-Foy, Quebec, Canada G1K 7P4

Received December 22, 1992; revised April 20, 1993

The synthesis of MAPO-36 molecular sieve was studied using different gel compositions and hydrothermal crystallization conditions. MAPO-36 is a large-pore molecular sieve which has a pore opening of 7.4 by 6.5 Å. Highly crystalline MAPO-36 molecular sieve was obtained by hydrothermal crystallization of the gel (molar composition: 1.8 Pr_3N–0.17 MgO–0.92 Al_2O_3–1.0 P_2O_5–40 H_2O) initially at 378 K for 50 h and finally at 423 K for 24 h. Increased concentration of organic template (tripropylamine) and metal (Mg) produced a decrease in the crystallinity of MAPO-36. Co-phase formation was observed in one particular case for decreased metal concentration. The N_2-, H_2O-, and *n*-hexane sorption capacity of MAPO-36 is higher than $AlPO_4$-5, which is due to the presence of the annular side-pockets in the crystal structure. SEM investigations of MAPO-36 crystals showed two different types of morphology. Thermal analysis of Pr_3N–MAPO-36 has been studied in the presence of inert and oxidizing atmospheres in the temperature range 303–1273 K. The removal of tripropylamine occluded in the channels of the material occurs in a number of steps and is strongly influenced by the gas atmospheres. XPS analysis indicated that the concentration of magnesium is higher on the surface than in the bulk of MAPO-36, and magnesium is tetrahedrally coordinated into the aluminophosphate framework. *In situ* IR spectroscopic investigation of chemisorbed pyridine on MAPO-36 revealed the presence of Brønsted and Lewis acid sites. Temperature-programmed desorption (TPD) of pyridine suggests that there exists a site energy distribution (which contains Lewis and Brønsted acid sites). By using GC techniques, TPD of pyridine at different initial sorbate loadings and stepwise thermal desorption (STD) of the base from 323 to 673 K were investigated. TPD of pyridine over MAPO-36 indicated the presence of two types of acid sites (with the majority being strong acid sites) and a significantly stronger acidity than $AlPO_4$-5, SAPO-5, and MAPO-5.

INTRODUCTION

A new generation of crystalline microporous aluminophosphate and metal aluminophosphate families has opened new horizons in catalytic fields due to the specificity of the different metal ions introduced into the framework or dispersed oxides occluded within zeolitic cages exhibiting unusual catalytic properties. Flanigen and co-workers (*1–4*) reported a series of different-element-substituted $AlPO_4$-based molecular sieves, which has extended the structural and composition varieties found among the growing number of $AlPO_4$-based molecular sieves. Synthesis and factors influencing the formation of pure metal-containing $AlPO_4$ and also metal and Si-containing $AlPO_4$ materials are reported (*5*). In MeAPO, both the metal and the organic template exert a primary influence on structure formation during synthesis. Moreover, MeAPO molecular sieves are interesting because the presence of metal in the framework also affects the ion-exchange and metal-specific behaviour of the material other than Brønsted acidity.

MAPO-36 reported by Flanigen *et al.* (*1*), has a unique three-dimensional structure with monoclinic symmetry (*6, 7*) and cell constants $a = 1.31$, $b = 2.16$, and $c = 0.52$ nm, and $\beta = 92°$. This material is characterized by a one-dimensional system of channels parallel to the *c*-axis with elliptical 12-ring apertures (pore diameter = 0.65 × 0.75 nm) and annular side-pockets. It is interesting to note that $AlPO_4$-5 and MAPO-36 can

0021-9517/93 $5.00

TABLE 1

Gel Composition and Synthesis Conditions for Pr_3N–MAPO-36 Molecular Sieve

Batch	Gel composition (Molar basis)	Syn. conditions		Product phase(s)	Crystallinity (%)[a]
		Temp. (K)	Period (h)		
A	1.8 Pr_3N · 0.17 MgO · 0.92 Al_2O_3 · 1.0 P_2O_5 · 40 H_2O · 0.33 HOAc	378 423	50 24	MAPO-36[A]	100
B	1.8 Pr_3N · 0.17 MgO · 0.92 Al_2O_3 · 1.0 P_2O_5 · 40 H_2O · 0.33 HOAc	378 423	50 12	MAPO-36[B] Amorph. (20%)	80
C	1.8 Pr_3N · 0.17 MgO · 0.92 Al_2O_3 · 1.0 P_2O_5 · 40 H_2O · 0.33 HOAc	423	24	MAPO-36[C] Amorph. (60%)	40
D	2.1 Pr_3N · 0.17 MgO · 0.92 Al_2O_3 · 1.0 P_2O_5 · 40 H_2O · 0.33 HOAc	378 423	50 24	MAPO-36[D] Amorph. (5%)	95
E	1.8 Pr_3N · 0.31 MgO · 0.85 Al_2O_3 · 1.0 P_2O_5 · 40 H_2O · 0.60 HOAc	378 423	50 24	MAPO-36[E] Amorph. (25%)	75
F	1.8 Pr_3N · 0.42 MgO · 0.80 Al_2O_3 · 1.0 P_2O_5 · 40 H_2O · 0.81 HOAc	378 423	50 24	MAPO-36[F]	70
G	1.8 Pr_3N · 0.06 MgO · 0.97 Al_2O_3 · 1.0 P_2O_5 · 40 H_2O · 0.12 HOAc	378 423	50 24	MAPO-5 (75%) MAPO-36[G]	25

[a] Crystallinity of MAPO-36 phase; Amorph.: Amorphous

be readily synthesized hydrothermally using only one type of template (tripropylamine), but in the former there is low template-structure specificity, while in the latter there is high template-structure specificity and the metal–template interaction influences the structure formation (*2, 8*).

MAPO-36 showed higher catalytic activity (*2, 9*) and acidity (*10*) among MAPO-5, SAPO-5, and $AlPO_4$-5. Pure crystalline MAPO-36 is difficult to prepare due to the cocrystallization of MAPO-5 and MAPO-36. The cocrystallization of the CoAPO-5 phase during the synthesis of CoAPO-36 was reported earlier (*5*). Therefore, the present investigation was undertaken to synthesize hydrothermally a pure phase of MAPO-36 and also to characterize it. The synthesis products were characterized by AAS, XRD, and SEM, and for their N_2- and H_2O-sorption capacity. Further, *n*-hexane sorption capacity, thermal analysis, and XPS measurements, and Brønsted and Lewis acid site distribution (*in situ* IR techniques) and site energy distribution (TPD and STD of pyridine using GC techniques) investigations were carried out on pure MAPO-36.

EXPERIMENTAL

Preparation of Pr_3N–MAPO-36

Pr_3N–MAPO-36 was synthesized by hydrothermal crystallization of reactive aluminophosphate gel containing Mg as the additional framework cation and tripropylamine (Pr_3N) as an organic template. The procedure followed was reported elsewhere (*2*). The reported procedure was used with certain modifications. The typical gel composition and synthesis conditions [Table 1: batch A] which gave pure Pr_3N–MAPO-36 are as follows: 1.8 Pr_3N–0.17 MgO–0.92 Al_2O_3–1.0 P_2O_5–40.0 H_2O–0.33 HOAc and hydrothermal treatment at 378 K for 50 h and further treatment at 423 K for 24 h. The other gel compositions and synthesis conditions for the preparation of Pr_3N–MAPO-36 are presented in Table 1. The sources of Al_2O_3, P_2O_5, and MgO were aluminium isopropoxide (Fluka), *ortho*-phosphoric acid [(85%) Merck, FRG], and magnesium acetate (Merck, FRG), respectively. The tri-

propylamine used was synthetic grade (Merck).

The typical gel mixture [batch A] was prepared as follows: (i) All the solid reactants were finely ground; (ii) 38.88 g aluminum isopropoxide was stirred in 35 g of deionised water at room temperature (299 K) for 15 min. A heavy duty overhead stirrer (motorized) with a high density polyethylene stirrer shaft with blades (blade dia. 44 mm) was used for mixing. (iii) Then 3.50 g of magnesium acetate [$Mg(CH_3COO)_2$ 4 H_2O] were dissolved in 15 g of water; (iv) 21 g of deionised water were added to 22.59 g of (85%) *ortho*-phosphoric acid. (v) The solution of magnesium acetate was added to the alumina source (i.e., aluminium isopropoxide slurry) (rate of addition of Mg acetate solution: 0.5 $cm^3\ min^{-1}$) with continuous stirring. (vi) The phosphoric acid solution was added (addition rate: 1 $cm^3\ min^{-1}$) to the alumina slurry to form a precursor mixture and it was stirred for 20 min; (vii) 27.1 g of tripropylamine was added at the rate of 0.5 $cm^3\ min^{-1}$ to the aluminophosphate-based gel with continuous stirring for 30 min at room temperature. The pH of the mixture was around 5. The gel was transferred into the stainless steel autoclave coated with teflon with a capacity of ca. 200 cm^3 and heated under static conditions initially at 378 K for 50 h and further heated at 423 K for 24 h. After the hydrothermal treatment, the observed pH of the product was about 8. The solid product obtained was processed by washing it with deionised water. The solid product was dried in an air oven at 373 K for 24 h. The organic template was removed from the material by calcination in the presence of air (flow rate: 100 $cm^3 \cdot min^{-1}$) at 813 K for 12 h. A similar procedure was adopted for preparing the other gel mixtures (Table 1) and for obtaining the products.

Characterization

The X-ray powder diffraction spectra were obtained by the Holland Philips PW/1730 X-ray generator with the Ni-filtered Cu$K\alpha$ radiation source and a scintillation counter. The atomic absorption spectroscopy and gravimetric analysis were used for the elemental analysis. The size and morphology of the crystals of MAPO-36 were studied using a JEOL JSM-840A scanning electron microscope. The N_2-sorption capacity data of the materials were obtained by N_2-dynamic adsorption/desorption technique (p/p_0 = 0.3) using a Quantasorb unit (Quantachrome Corp., U.S.A) and the H_2O- and *n*-hexane sorption capacity were determined gravimetrically (*11*).

For thermal analysis, Pr_3N–MAPO-36[A] dried at 373 K in air for 16 h was used. Thermal analysis (TG/DTG/DTA) data on Pr_3N–MAPO-36 were obtained under inert and oxidizing atmospheres, using fully automated and computer-assisted TG/DTA 220 simultaneous Thermogravimetric/Differential Thermal Analyzer (Seiko Instruments, Inc., Japan) under the following conditions: sample size, 20 mg; reference compound, α-alumina; sample holder, platinium crucible; temperature range, 301–1211 K; heating rate, 10 deg min^{-1}; atmosphere, flowing air or nitrogen (flow rate, 100 $cm^3\ min^{-1}$).

XPS measurements were conducted for determining the surface concentration and binding energy of O_{1s}, Mg_{2p}, Al_{2p}, and P_{2p}. A V.G. Scientific Escalab Mark II system with a hemispherical analyzer operated in the constant pass energy mode (20 eV) was employed. An Mg$K\alpha$ X-ray source ($h\nu$ = 1253.6 eV) was operated at 20 mA and 15 kV. The intensity of the XPS band was determined using linear background subtraction and integration of peak areas.

The IR spectrum of Pr_3N-MAPO-36[A] in the lattice vibration range (1400–400 cm^{-1}) (see Fig. 4) was obtained with 2-cm^{-1} resolution using a Digilab-FTS-60 spectrometer. The sample was examined in the form of a KBr disc with 1.3 mg of sample in 100 mg of KBr. The *in situ* acidity measurements were performed on a self-supported wafer (15 mg) (thickness, 10.0 mg cm^{-2}) using an infrared spectrometer (IR-580B, Perkin–Elmer, U.S.A.). The MAPO-36 wafer

was first activated *in situ* in the presence of a mixture of He and O_2 (20%) at 825 K for 5 h and further in vacuum (5×10^{-7} mbar) at 798 K for 5 h. Freshly distilled pyridine was adsorbed at 473 K for 2 h by contacting the vapour of the liquid at 273 K (0.12 mbar) and subsequently, pyridine was desorbed at 473 K for 1 h under 10^{-6} mbar. To investigate Brønsted and Lewis acid site distribution, TPD of pyridine was carried out in an ultrahigh vacuum apparatus used in an IR spectrometer. TPD was carried out from 473 to 873 K at a linear rate of 20 K min^{-1}. Brønsted and Lewis acid sites were determined on the basis of the absorbance of the PyB band near 1543 cm^{-1} and the PyL band near 1447 cm^{-1}, respectively.

The site energy distribution of MAPO-36 was measured by TPD of pyridine at different initial sorbate loadings (heating rate 5 K min^{-1}) and also by STD of pyridine using the GC techniques. The procedure for the measurement of chemisorption and STD of pyridine and also for evaluating the chemisorption data from STD are reported (*12–15*).

RESULTS AND DISCUSSION

Synthesis of Pr_3N–MAPO-36

For the preparation of highly crystalline MAPO-36 molecular sieve, different types of gel compositions and synthesis conditions were employed (Table 1). In batches [A], [B], and [C], the gel composition was kept constant; only the synthesis conditions were changed. When the gel was hydrothermally crystallized at 378 K for 50 h and finally at 423 K for 24 h, highly crystalline MAPO-36[A] {batch [A]} was produced. By reducing the final crystallization period from 24 to 12 h {in batch [B]}, MAPO-36[B] was obtained with lower crystallinity (80%). In batch [C], MAPO-36[C] was formed only with 40% crystallinity when the gel was directly hydrothermally crystallized at 423 K for a period of 24 h. The results show that the formation of MAPO-36 crystals could take place at 378 K {batches [A] and [B]} and at 423 K {batch [C]}, however, the crystallinity is decreased by reducing the crystallization period in the second stage. This suggests that in the second stage {423 K and 24 h; batches [A] and [B]} of synthesis, further growth of MAPO-36 crystals occurs. Direct crystallization of the gel at 423 K for 24 h gave MAPO-36[C] with very low crystallinity. To see the effect of the concentration of organic template on the crystallinity, tripropylamine concentration was increased by 16% in batch [D] and the synthesis conditions were same as those of batch [A]. Crystalline product {MAPO-36[D]} with 95% crystallinity was obtained, though the higher gel–Pr_3N level is effective in favouring the 36 structure. The results indicate that the gel composition and synthetic conditions of batch [A] are optimum and suitable for obtaining pure MAPO-36 material. Efforts were made to introduce higher amounts of Mg in MAPO-36 in batches [E] and [F]. However, the crystallinity of the products {MAPO-36[E] and MAPO-36[F]} was quite low as compared to that of MAPO-36[A]. The lower crystallinity of MAPO-36[E] and MAPO-36[F] materials may be because of the formation of nonmicroporous Mg-rich structures (at higher Mg concentrations) as reported earlier (*2*). By decreasing the Mg concentration in the gel {batch [G]}, two phases of aluminophosphate (type 5 and 36) were obtained, which indicates that the lower concentration of Mg in the gel does not help to obtain pure MAPO-36 phase.

Characterization

Figure 1 shows the powder XRD spectrum of Pr_3N-MAPO-36[A] which is very similar to that for MAPO-36 reported earlier (*2*). The crystalline nature and crystallinity of the synthesized products are presented in Table 1.

The elemental analysis of MAPO-36[A] obtained by atomic absorption spectroscopy and gravimetric analysis is $(0.04\ Mg–0.46\ Al–0.50\ P)O_2$. Since MAPO-36[A] was highly crystalline, this sample was used for characterization and catalytic properties studies (*9*). The elemental analysis of MAPO-36 shows that there are no extraneous Al or P or Mg elements present in the

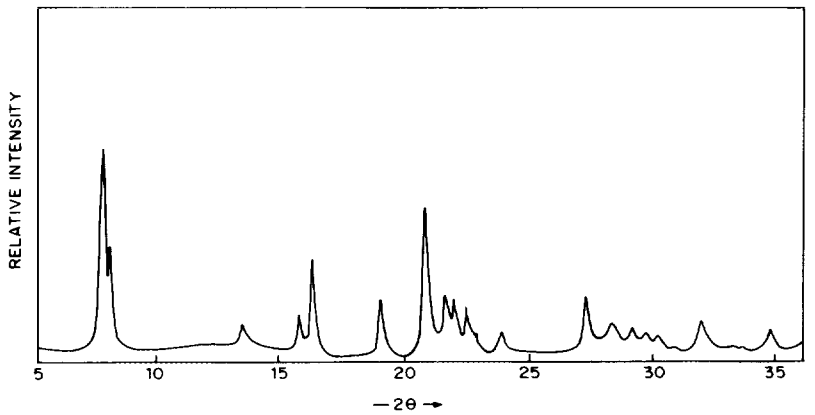

FIG. 1. X-ray powder diffraction pattern of Pr_3N–MAPO-36[A] molecular sieve.

framework and Mg substitutes for some of the Al in the aluminophosphate framework. According to the elemental analysis, the sum of the atomic fractions of magnesium and aluminium, and of phosphorus equals 0.5. So the general rules outlined by Flanigen *et al.* (*3*) seem to be obeyed by MAPO-36. Hence Mg seems to be exclusively incorporated into Al-sites only via a type 1 mechanism. In the metal aluminophosphate framework, magnesium bonds phosphorus via oxygen such as –O–P–O–Mg–O–P–. The framework charge calculated from the chemical composition of MAPO-36 is −0.04 electron/T atom which is in the range for those of MeAPO-*n* reported elsewhere (*3*).

The N_2- and H_2O-sorption capacity of the metal aluminophosphates are presented in Table 2. MAPO-36[A] shows higher N_2-sorption capacity (5.5 mmol g^{-1}) and H_2O-sorption capacity (17.18 mmol g^{-1}) than the other metal aluminophosphates {MAPO-36[B–G]}. The *n*-hexane sorption capacity of MAPO-36[A] is 0.20 $cm^3\ g^{-1}$ (1.51 mmol g^{-1}) at 296 K. MAPO-36[A] possesses higher N_2-, H_2O-, and *n*-hexane sorption capacity than $AlPO_4$-5 (*11*), which is due to the presence of annular side-pockets in the crystal structure (*7*). The result that the N_2-, H_2O-, and *n*-hexane sorption capacities of MAPO-36 are higher than that of $AlPO_4$-5 is consistent with the O_2- and H_2O- adsorption

TABLE 2

N_2- and H_2O-sorption Capacity of the Crystalline Product Obtained Using Different Gel Composition and Synthesis Conditions

Batch	Product	N_2-sorption capacity at 78 K (p/p_0 = 0.3) (mmol · g^{-1})	H_2O-sorption capacity at 296 K (mmol · g^{-1})
A	MAPO-36[A]	5.56	17.18
B	MAPO-36[B]	4.51	14.51
C	MAPO-36[C]	2.6	8.86
D	MAPO-36[D]	5.15	16.20
E	MAPO-36[E]	4.18	13.42
F	MAPO-36[F]	3.62	12.14
G	MAPO-36[G]	4.21	10.45
[a]	$AlPO_4$-5	4.86	12.02

[a] Ref. (*11*).

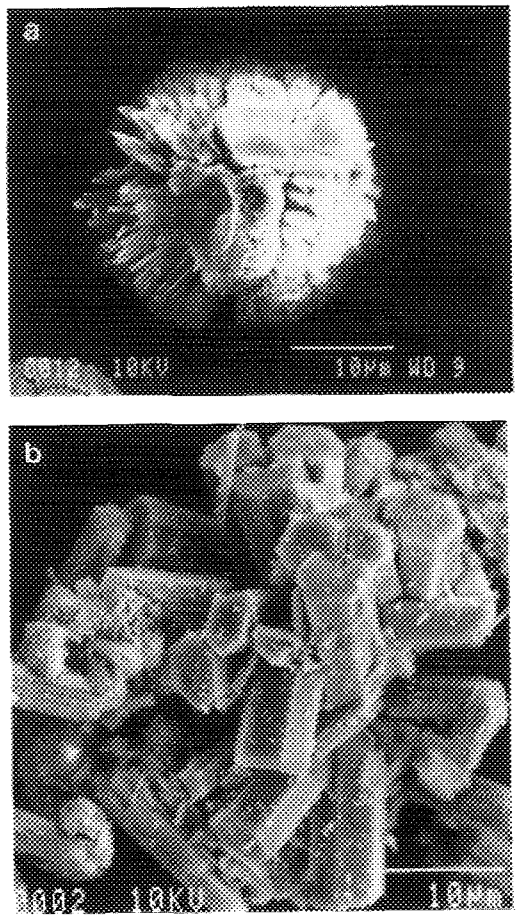

FIG. 2. Typical scanning electron photomicrographs of (a) Pr_3N–MAPO-36[D] and (b) Pr_3N–MAPO-36[A] molecular sieve.

capacity results of MAPO-36 reported earlier (*2*).

Figure 2 shows the scanning electron photomicrographs of Pr_3N-MAPO-36 {batches [A] and [D]}. SEM studies of these materials reveal the presence of two types of morphology. In the case of Pr_3N–MAPO-36[D], the crystals are thin, needle/rod-like, and attached to a sphere. The approximate length of the thin rod-like crystals is 12 μm. These types of crystals were also observed in the [B], [E], and [F] batches, while in the case of Pr_3N–MAPO-36[A] {Fig. 2b} the crystals are hexagonal rod-like with average size of 5.5 × 11 μm. According to the observations, these hexagonal rod-like crystals are formed in the spherical particle. When the crystals are fully grown they fall out of the spherical particle.

Figure 3 shows the TG, DTG, and DTA curves for the decomposition of Pr_3N–MAPO-36[A] in nitrogen (a) and in air (b). The TG, DTG, and DTA data of Pr_3N–MAPO-36[A] in different gas atmospheres are presented in Table 3. From the TG and DTG data it follows that there are four distinct steps of weight loss from MAPO-36 containing tripropylamine in inert and oxidizing atmospheres.

The results of TG/DTG/DTA indicate that in an inert atmosphere most of the processes occurring in the removal of occluded materials from the metal-aluminophosphate are endothermic. The total weight loss

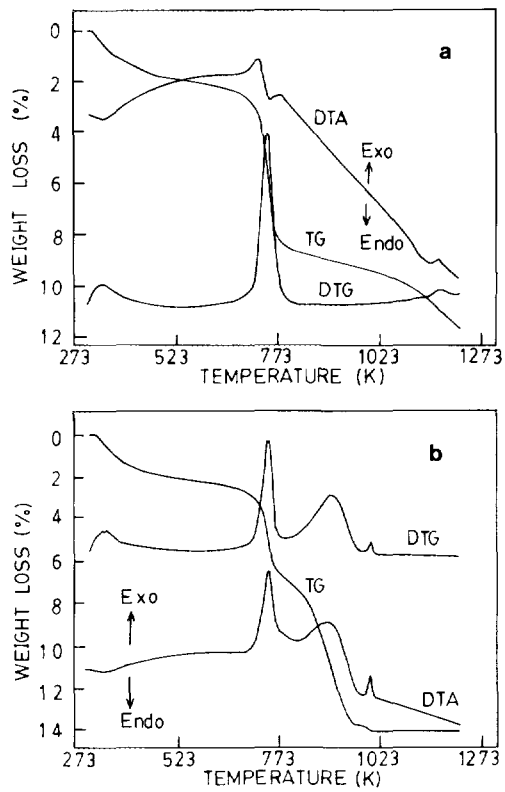

FIG. 3. TG, DTG, and DTA curves for the decomposition of Pr_3N–MAPO-36[A] in nitrogen (a) and in air (b).

TABLE 3

TG, DTG, and DTA data of Pr_3N–MAPO-36[A] in Different Gas Atmospheres

Decomp. stage	Nitrogen					Air				
	Temp. range (K)	Wt. loss (%)	Total wt. loss (%)	Peak temp. (K)		Temp. range (K)	Wt. loss (%)	Total wt. loss (%)	Peak temp. (K)	
				DTG	DTA				DTG	DTA
I	301–567	1.9	1.9	336	334 (Endo)	301–573	2.3	2.3	338	338 (Endo)
II	567–798	6.7	8.6	730	672 (Endo) 748 (Exo)	573–761	4.3	6.6	739	746 (Exo)
III	798–1067	1.3	9.9	—	—	761–948	7.1	13.7	898	891 (Exo)
IV	1067–1211	1.8	11.7	1161	1139 (Endo) 1164 (Exo)	948–1211	0.2	13.9	996	998 (Exo)

amounts to 11.7 wt% in an inert atmosphere. In the first stage, the weight loss is 1.9 wt% at 301–567 K, which is due to the desorption of physisorbed water and tripropylamine from the metal-aluminophosphate. The major weight loss (6.7 wt%) occurs in the second stage at 567–798 K, particularly in the narrow range 717–798 K. The second stage corresponds to the desorption of tripropylamine and possibly to cracking of the occluded tripropylamine molecules to smaller molecules. This decomposition is also consistent with the behaviour of amine containing ZSM-5 precursors (*16*) and tripropylamine containing aluminophosphate (*17*). In the third stage, the weight loss of 1.3 wt% occurs at 798–1067 K, which is due to the very slow desorption of ammonia and/or tripropylamine adsorbed strongly on the high energy sites in MAPO-36[A]. Current investigations on TPD of pyridine also indicated the presence of high-energy sites on MAPO-36. In the fourth stage (1067–1211 K) a small weight loss (1.8 wt%) is mostly due to the very slow desorption of ammonia and/or tripropylamine adsorbed strongly on the high-energy sites of the MAPO-36. Also a fraction of the weight loss (ca. 0.5 wt%) is exothermic in nature, which is due to the release of trapped gaseous products after complete collapse of the structure (*5*). Our recent investigations on the thermal stability of MAPO-36 (*18*) revealed that the complete collapse of the structure occurs above 1113 K.

In an oxidizing atmosphere, TG/DTG/DTA results indicate that the decomposition in the presence of air is a very complex process which occurs in four distinct stages with a total weight loss of 13.9 wt%. In the first stage, the desorption of physisorbed water and tripropylamine from Pr_3N–MAPO-36 occurs at lower temperatures (301–573 K) and the weight loss is 2.3 wt%. In the second and third stages, a major weight loss occurs at 573–761 K and 761–948 K, respectively. The fourth weight loss (0.2 wt%) occurs at 948–1211 K. In these stages, the removal of tripropylamine is expected to be mostly due to its oxidative decomposition, which is an exothermic process. The oxidative decomposition is thought to involve the thermal cracking of the occluded tripropylamine, followed by oxidation of the cracking products in the intra- and intercrystalline spaces and also the direct oxidation of tripropylamine within the channels.

The surface concentration of the elements on the calcined MAPO-36[A] determined by XPS measurements is O_{1s}, 61.22%; Mg_{2p}, 3.86%; Al_{2p}, 16.77%; and P_{2p}, 18.14%. Bulk and surface composition and XPS binding energy data for MAPO-36[A] are presented in Table 4. The higher value of Mg/Al ratio indicates that the concentration of magne-

TABLE 4

XPS Results for MAPO-36[A]

Binding energy (eV)/FWHM (eV)[a]				Atomic ratio			
				Mg/Al		Al/P	
Al_{2p}	P_{2p}	Mg_{2p}	O_{1s}	Bulk	Surface	Bulk	Surface
74.1(2.0)	134.3(2.6)	50.4(2.4)	532(2.5)	0.09	0.23	0.92	0.92

[a] Referenced to $Au_{4f7/2}$ = 84.0 eV.

sium on the surface of MAPO-36[A] is higher. While the Al/P ratio which is approximately same indicates the similar concentration of aluminium and phosphorous present on the surface and in the bulk of MAPO-36[A]. The binding energy measured for Mg_{2p} in MAPO-36[A] is 50.4 eV. This value is very close to the one reported for tetrahedrally coordinated Mg in the spinel structure $MgAl_2O_4$ (*19, 20*). It is, therefore, concluded that the observed Mg_{2p} line in MAPO-36[A] is for the tetrahedrally coordinated Mg in the lattice.

The IR spectrum of Pr_3N–MAPO-36[A] is shown in Fig. 4. *In situ* infrared spectra after desorption of pyridine at 473 K from MAPO-36 pretreated at 798 K is shown in Fig. 5. The bands at 1447, 1492, and 1543 cm^{-1} are ascribed to Lewis, Lewis and/or Brønsted, and Brønsted acid sites, respectively (*21*). These show the presence of Brønsted and Lewis acid sites on MAPO-36. As such, the crystalline aluminophosphate molecular sieve consists of alternating alumina and phosphate tetrahedra and so is electronegatively neutral with no extra-framework cations and no ion-exchange capacity. In metal aluminophosphate, the metal cations (Me^{2+}) are incorporated into the aluminophosphate framework substituting for Al^{3+} hypothetically (*1*) resulting metal aluminophosphate framework with negative charge. This negative charge must be balanced by protons or metal cations,

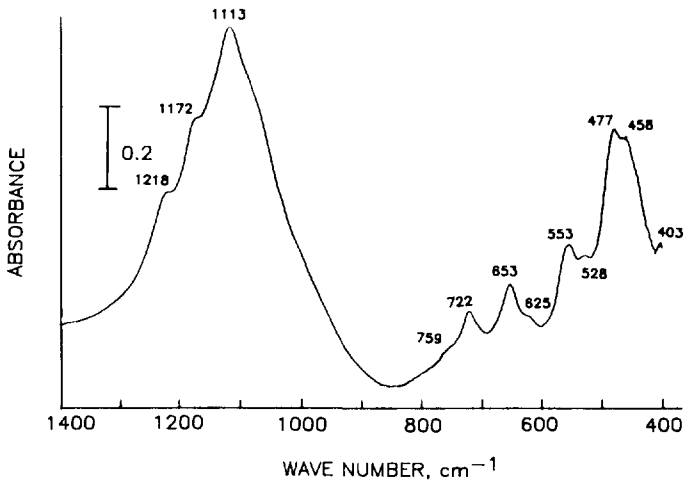

FIG. 4. IR spectrum of Pr_3N–MAPO-36[A].

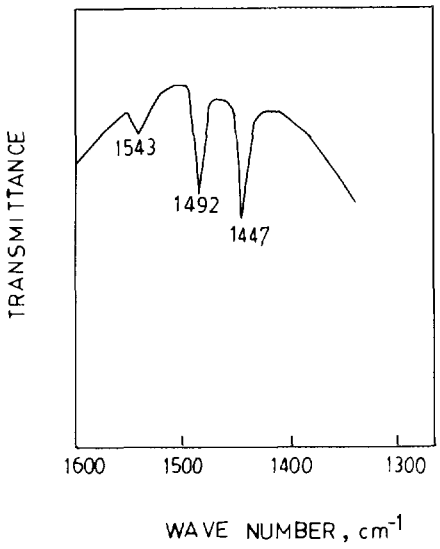

FIG. 5. *In situ* infrared spectrum of chemisorbed pyridine on MAPO-36[A] molecular sieve (pyridine chemisorbed at 473 K).

resulting in Brønsted acidity or ion-exchange capacity. Likewise in MAPO-36 framework Al^{3+} is replaced by Mg^{2+} giving rise to a negatively charged metal aluminophosphate framework which further leads to development of Brønsted acidity or ion-exchange capacity.

The distribution of Brønsted and Lewis acid sites on MAPO-36[A] (Fig. 6) is obtained by temperature-programmed desorption of pyridine carried out in an ultrahigh vacuum apparatus combined with an IR-spectrometer. The results indicate a clear distribution of Brønsted and Lewis acid sites on MAPO-36[A]. The metal aluminophosphate molecular sieve possesses a higher number of Lewis acid sites than Brønsted acid sites. The numerical ratios of Brønsted to Lewis acid sites at 473, 573, 673, 723, and 773 K are 0.29, 0.37, 0.21, 0.58, and 0.43, respectively. The ratio of Brønsted to Lewis acid sites is highest at 723 K. The distribution of Brønsted and Lewis acid sites on MAPO-36 is found to be broad. Composition of Brønsted and Lewis acidity results indicate that MAPO-36[A] possesses higher acidity than $AlPO_4$-5, SAPO-5, and MAPO-5 (SAPO-5 and MAPO-5 containing an amount of substituted element equivalent to that of Mg in MAPO-36[A]) at 473 K (*10, 22, 23*).

The TPD chromatograms on MAPO-36[A] at a heating rate of 5 K min^{-1} and different initial concentrations (θ_i) of pyridine are presented in Fig. 7. In the TPD chromatograms two peaks are observed, which indicates the involvement of two types of active site in the desorption process. The desorption appears to be first order, as the chromatograms are asymmetric. The peak maximum temperature (T_m) (of the first peak) for the desorption is shifted toward the higher temperature side with a decrease in the value of θ_i (up to 49 μmol g^{-1}), which indicates the presence of a site energy distribution on MAPO-36.

The values of T_m for the two peaks at different initial sorbate loadings are given

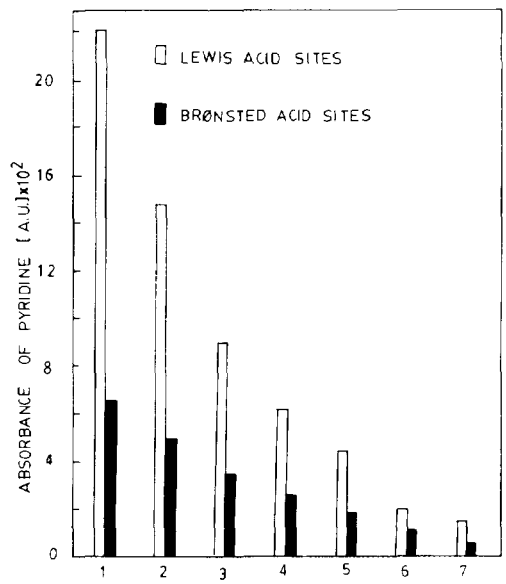

FIG. 6. Distribution of Brønsted and Lewis acid sites on MAPO-36[A] molecular sieve: (1) 473 K, (2) 523 K, (3) 573 K, (4) 623 K, (5) 673 K, (6) 723 K, and (7) 773 K.

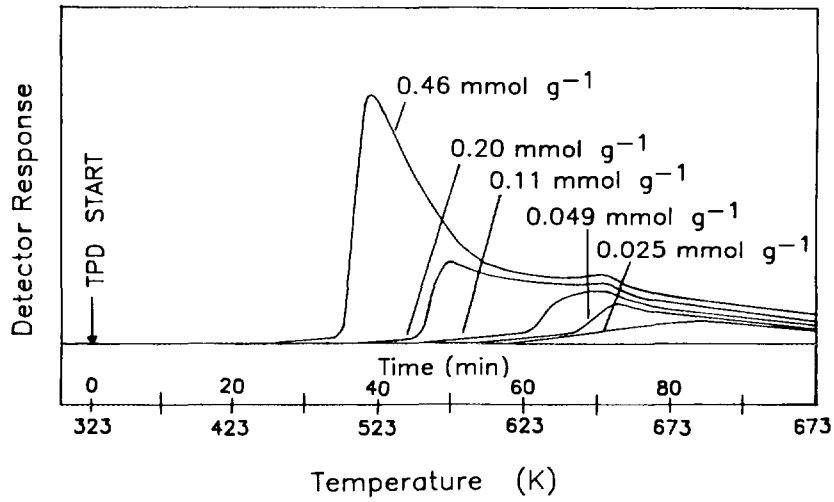

FIG. 7. TPD chromatograms of pyridine on MAPO-36[A] (amount of catalyst: 0.26 g; He-flow rate, 10 cm^3 min^{-1}; heating rate, 5 K min^{-1}).

below:

θ_i (μmol g^{-1}):	460	200	110	49	25
T_m (K) Peak 1:	513	567	649	673	673
T_m (K) Peak 2:	673	673	673		

By increasing the heating rate (10 K min^{-1}), a shift in the peak maximum temperature (567 K) of the first peak at initial sorbate loading of 350 μmol g^{-1} is observed. The peak maximum temperature (673 K) of the second peak is unaffected. The site energy distribution obtained from the STD of pyridine on MAPO-36[A] is shown in Fig. 8. The strength of the site involved in the pyridine chemisorption is expressed in terms of the desorption temperature (T_d), which lies in the range of temperatures in which the chemisorbed pyridine is desorbed. Here, T_d^* is the measure of the maximum strength possessed by the site and corresponds to the temperature at which the pyridine chemisorbed on the strongest sites is desorbed. The columns in the figure show the strength distribution of the sites (equivalent to 0.10 mmol g^{-1}) involved in the chemisorption at the lowest temperature of the STD (i.e.,

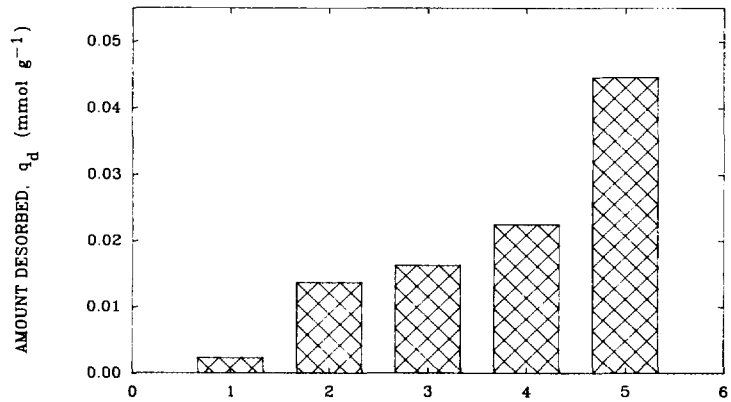

FIG. 8. Site energy distribution on MAPO-36[A]: (1) 323 K < T_d < 373 K, (2) 373 K < T_d < 473 K, (3) 473 K < T_d < 573 K, (4) 573 K < T_d < 673 K, and (7) 673 K < T_d < T_d^*.

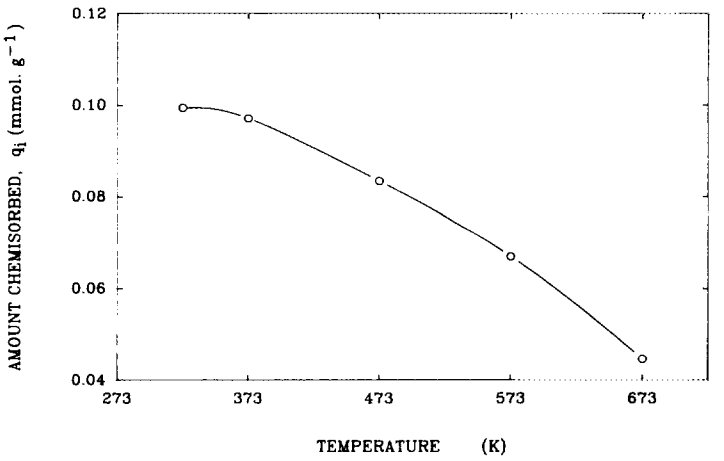

FIG. 9. Temperature dependence of chemisorption of pyridine on MAPO-36[A].

323 K). The sites of strength 673 K $< T_d \leq T_d^*$ were obtained from the amount of pyridine chemisorbed at 673 K. On the other hand, the sites of strength $T_1 < T_d \leq T_2$ were obtained from the amount of pyridine which was initially chemisorbed at T_1 but desorbed by increasing the temperature to T_2.

Figure 9 shows the temperature dependence of the chemisorption of pyridine on the aluminophosphate. The chemisorption data were obtained from the STD data by the procedure described earlier (*12, 15*). The chemisorption of pyridine at higher temperatures points to the involvement of the stronger sites. The q_i vs T curve, therefore, presents a type of site energy distribution in which the number of sites are expressed in terms of the amount of pyridine chemisorbed as a function of the sorption temperature.

The results on the TPD and STD of pyridine have clearly shown that there exists a site energy distribution on MAPO-36[A] and the distribution is broad. It is interesting to note that MAPO-36[A] contains fewer weak acid sites and the majority of sites are stronger ones. This is confirmed by the extraordinary catalytic activity shown by MAPO-36 (*9*), as compared to the other aluminophosphates of type 5 (e.g., $AlPO_4$-5, SAPO-5, MAPO-5) in the acid-catalyzed reactions such as the cracking of hydrocarbons (pentane, 3-methyl-pentane, *n*-hexane, iso-octane, cyclohexane, cumene), *o*-xylene isomerization, toluene disproportionation, and the aromatization in methanol and ethanol conversion reactions.

CONCLUSIONS

Highly crystalline MAPO-36 was obtained by hydrothermally crystallizing a gel of composition 1.8 Pr_3N–0.17 MgO–0.92 Al_2O_3–1.0 P_2O_5–40 H_2O initially at 378 K for 50 h and finally at 423 K for 24 h. The preparation of pure MAPO-36 in the presence of tripropylamine is restricted to a very narrow range of gel composition.

MAPO-36 possesses higher N_2-, H_2O-, and *n*-hexane sorption capacity than $AlPO_4$-5, which is due to the presence of the annular side-pockets in the crystal structure. Thermal analysis results indicate that in an inert atmosphere most of the processes occurring in the removal of occluded tripropylamine from the metal aluminophosphate are endothermic. In an oxidizing atmosphere, the thermal analysis results indicate that the decomposition is mostly exothermic and strongly influenced by the presence of oxygen. In both the cases, the decomposition occurs in four distinct stages. The TG/DTG/DTA investigations indicate that a

calcination temperature of 813 K is sufficient for the removal of occluded tripropylamine from Pr_3N–MAPO-36.

The results of the bulk and surface composition of MAPO-36[A] indicate that the concentration of magnesium is higher on the surface. The observed binding energy of Mg_{2p} (50.4 eV) in MAPO-36 suggests that the magnesium is tetrahedrally coordinated into the aluminophosphate framework.

In situ IR studies on MAPO-36 show that it possesses Brønsted and Lewis acid sites. Generation of Brønsted acid sites on MAPO-36 is attributed to an anionic framework charge developed by incorporation of Mg into the hypothetical Al sites. The results of TPD of pyridine on MAPO-36 showed the distribution of Lewis and protonic acid sites.

TPD and STD of pyridine over MAPO-36 show the presence of a site energy distribution. The weak acid sites are fewer in number on MAPO-36 and the majority are strong acid sites. The number of strong acid sites on MAPO-36 is very much higher than that on $AlPO_4$-5, SAPO-5, and MAPO-5.

ACKNOWLEDGMENTS

The author is sincerely thankful to Dr. H.G. Karge, Fritz Haber Institute of the Max Planck Society, Berlin, Germany, for providing the experimental and helpful discussions. The author is grateful to the Alexander von Humboldt Foundation, Bonn, Germany, for an award of an international research fellowship.

REFERENCES

1. Flanigen, E. M., Lok, B. M., Patton, R. L., and Wilson, S. T., *in* "Proceedings, 7th International Zeolite Conference, Tokyo, Japan, 1986" (Y. Murakami, A. Iijima, and J. W. Ward, Eds). p. 103. Kodansha, Tokyo, 1986.
2. Wilson, S. T., and Flanigen, E. M., *ACS Symp. Ser.* **398,** 329 (1989).
3. Flanigen, E. M., Patton, R. L., and Wilson, S. T., *in* "Innovation in Zeolite Material Science" (P. J. Grobet, W. J. Mortier, E. F. Vansant, and G. Schulz-Ekloff, Eds.), Stud. in Surf. Sci. and Cat., Vol. 37, p. 13. Elsevier, Amsterdam, 1988.
4. Wilson, S. T., Lok, B. M., Messina, C. A., and Flanigen, E. M., *ACS Symp. Ser.* **218,** 79 (1983).
5. Ernst, S., Puppe, L., and Weitkamp, J., *in* "Zeolites: Facts, Figures, Future" (P. A. Jacobs and R. A. van Santen, Eds.), Stud. in Surf. and Cat., Vol. 49, p. 447. Elsevier, Amsterdam, 1989.
6. Smith, J. V., Pluth, J. J., and Andries, K. J., *in* "Atlas of Zeolite Structure Types" (W. M. Meir and D. H. Olson, Eds.), 3rd revised ed., p. 50. Butterworth–Heinemann, London, (1992).
7. Smith, J. V., Pluth, J. J., and Andries, *Zeolites,* **13,** No. 3, 166 (1993).
8. Derouane, E. G., and von Ballmoos, R., Eur. Patent Appls. 0146385–0146390 (1985).
9. Akolekar, D. B., *J. Catal.*, in press.
10. Akolekar, D. B., submitted for publication.
11. Choudhary, V. R., Akolekar, D. B., Singh, A. P., and Sansare, S. D., *J. Catal.* **111,** 23 (1988).
12. Choudhary, V. R., *J. Chromatogr.* **268,** 207 (1983).
13. Akolekar, D. B., and Choudhary, V. R., *J. Catal.* **105,** 416 (1987).
14. Choudhary, V. R., and Nayak, V. S., *Appl. Catal.* **4,** 31 (1982).
15. Nayak, V. S., and Choudhary, V. R., *J. Catal.* **81,** 26 (1983).
16. Parker, L. M., Bibby, D. M., and Patterson, J. E., *Zeolites* **4,** 168 (1984).
17. Choudhary, V. R., and Sansare, S. D., *J. Thermal Anal.* **32,** 777 (1987).
18. Akolekar, D. B., unpublished work.
19. Tossell, J. A., *J. Am. Chem. Soc.* **97,** 4840 (1975).
20. Haycock, D. E., Nicholls, C. J., Urch, D. S., Webber, M. J., and Wiech, G., *J. Chem. Soc. Dalton Trans.*, 1785 (1978).
21. Ward, J. W., *in* "Zeolites Chemistry and Catalysis" (J. A. Rabo, Ed.), Vol. 171, p. 118. ACS Monograph, Washington, DC, 1976.
22. Choudhary, V. R., and Akolekar, D. B., *J. Catal.* **103,** 115 (1987).
23. Akolekar, D. B., submitted for publication.